

# Recognition of Images Degraded by Gaussian Blur

Jan Flusser, *Senior Member, IEEE*, Sajad Farokhi, Cyril Höschl IV, Tomáš Suk,  
Barbara Zitová, and Matteo Pedone

**Abstract**—In this paper, we propose a new theory of invariants to Gaussian blur. We introduce a notion of a primordial image as a canonical form of all Gaussian blur-equivalent images. The primordial image is defined in spectral domain by means of projection operators. We prove that the moments of the primordial image are invariant to Gaussian blur and we derive recursive formulas for their direct computation without actually constructing the primordial image itself. We show how to extend their invariance also to image rotation. The application of these invariants is in blur-invariant image comparison and recognition. In the experimental part, we perform an exhaustive comparison with two main competitors: 1) the Zhang distance and 2) the local phase quantization.

**Index Terms**—Blurred image, object recognition, blur invariant comparison, Gaussian blur, projection operators, image moments, moment invariants.

## I. INTRODUCTION

IMAGE recognition/classification in general is an extremely broad area which apparently cannot be resolved by a single, always-optimal method. This is why numerous specific formulations of the problem have appeared, which consequently has resulted in many approaches and particular algorithms. Some of them have already become an established discipline of image analysis while some others are still undergoing initial development. One of the representatives of the latter group are methods for recognition of images which are degraded by a uniform Gaussian blur.

Few years ago, this task was considered a borderline problem. Thanks to the rapid development of imaging sensors and technologies that are nowadays available everywhere, the challenge of recognizing Gaussian-blurred images has started to appear more and more often in practice which consequently has attracted the attention of the researchers.

The mathematical formulation of the problem is well known in image processing. Capturing an ideal scene  $f$  by an imaging

device with the point-spread function (PSF)  $h$ , the observed image  $g$  is a convolution of both

$$g(x, y) = (f * h)(x, y). \quad (1)$$

This linear space-invariant image formation model, even if it is very simple, is a reasonably accurate approximation of many imaging devices and acquisition scenarios. In this paper, we concentrate our attention to the case when the PSF is a Gaussian function with unknown parameters.

Gaussian blur appears whenever the image was acquired through a turbulent medium and the acquisition/exposure time is by far longer than the period of Brownian motion of the particles in the medium. Ground-based astronomical imaging through the atmosphere, taking pictures through a fog, underwater imaging, and fluorescence microscopy are typical examples of such situation (in some cases, the blur may be coupled with a contrast decrease). Gaussian blur is also introduced into the images as the sensor blur which is due to a finite size of the sampling pulse; this effect is, however, mostly of low significance. Moreover, Gaussian kernel is often used as an approximation of some other blurs which are too complicated to work with them exactly. Gaussian blur is sometimes even introduced into the image intentionally, for instance to suppress additive noise, to “soften” the image or to perform local averaging before the image is down-scaled (see Fig. 1 for some examples). Numerous examples of the Gaussian convolution can be found outside the image processing area – particle transportation, diffusion process, time-development of a heat distribution in a mass, and photon scattering in radiation physics are few examples. Most of them are represented by 2D or 3D functions which can be visualized, that brings us back to image processing. So, we can see there is actually a demand for developing the tools designed particularly for processing Gaussian-blurred images.

When we need to classify a blurred image  $g$  against a database of clear images, we have basically three options. The most time-expensive one is to generate all possible blurred versions of all templates (i.e. blurring with Gaussians the variances of which fill a reasonable, properly sampled interval) and incorporate them into the database. This brute-force approach is not practically feasible. Another approach relies on the solution of the inverse problem, when the blur is removed from the input image and the deblurred image is then classified by any standard technique. This process contains semi-blind image deconvolution (the term “semi-blind” is used because we know the parametric form of the kernel but its parameters are unknown) which is in the case of a Gaussian kernel an unstable, ill-posed problem. Unlike motion blur and out-of-focus blur, Gaussian blur does

Manuscript received April 7, 2015; revised July 29, 2015 and October 18, 2015; accepted December 14, 2015. Date of publication December 23, 2015; date of current version January 7, 2016. This work was supported by the Czech Science Foundation under Grant GA15-16928S. The associate editor coordinating the review of this manuscript and approving it for publication was Prof. Dacheng Tao.

J. Flusser, C. Höschl IV, T. Suk, and B. Zitová are with the Institute of Information Theory and Automation, Czech Academy of Sciences, Prague 182 08, Czech Republic (e-mail: flusser@utia.cas.cz; hoschl@utia.cas.cz; suk@utia.cas.cz; zitova@utia.cas.cz).

S. Farokhi is with the Institute of Information Theory and Automation, Czech Academy of Sciences, Prague 182 08, Czech Republic, and also with the Faculty of Computer Engineering, Najafabad Branch, Islamic Azad University, Najafabad 85141-43131, Iran (e-mail: fsajad2@utia.cas.cz).

M. Pedone is with the Center for Machine Vision Research, Department of Computer Science and Engineering, University of Oulu, Oulu FI-90014, Finland (e-mail: matped@ee.oulu.fi).

Color versions of one or more of the figures in this paper are available online at <http://ieeexplore.ieee.org>.

Digital Object Identifier 10.1109/TIP.2015.2512108

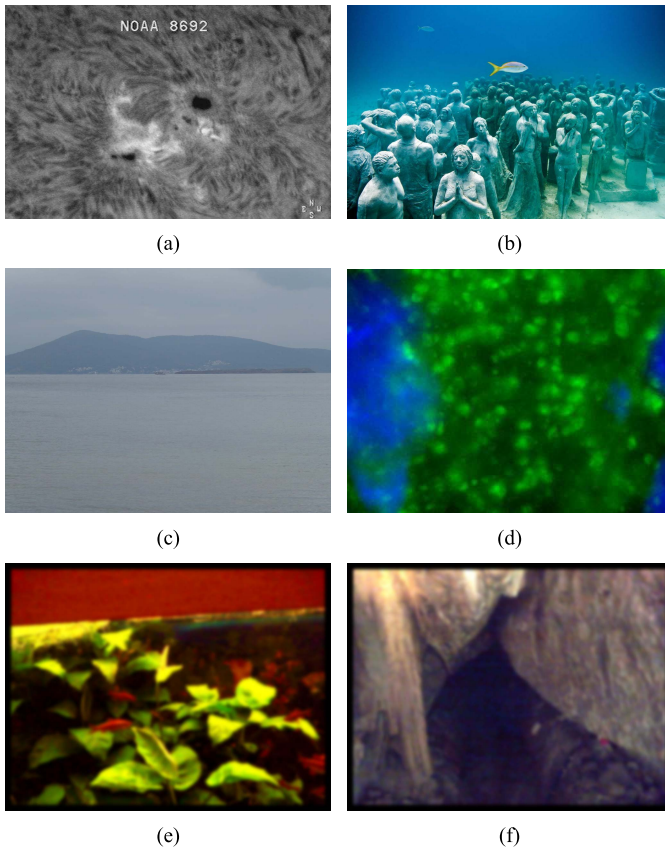


Fig. 1. Examples of the Gaussian blur: (a) the image of the sunspot blurred by atmospheric turbulence, (b) the underwater photo blurred by light dispersion, (c) a picture blurred due to a fog, (d) the image of axon boutons from wide-field epifluorescence microscopy, (e) the snap of an aquarium and (f) the snap from the cave. The last two pictures were originally very noisy because of poor light conditions, the noise was suppressed by applying a computer-generated Gaussian blur.

not introduce any zero patterns into the spectrum of the image, which are in the other cases employed for parameter estimation. Another difficulty is that the Gaussian can be factorized into an arbitrary (theoretically infinite) number of convolution terms, each of them being again a Gaussian. Hence, deconvolution algorithms cannot in principle remove Gaussian blur if no prior information is available. If the blur size (i.e. the variance of the Gaussian) was known, then we could apply a convolution with an inverse kernel (which can be synthesized by Hermite polynomials) or Wiener deconvolution in the frequency domain to deblur the image. Unfortunately, in image processing this scenario is not realistic because the blur size uses to be unknown, which makes the deblurring difficult. Only few semi-blind deconvolution methods w.r.t. Gaussian blur have been published. They first try to estimate the size (variance) of the blur and perform a non-blind deconvolution. Honarvar *et al.* [1] and Honarvar and Flusser [2] proposed to perform the deconvolution in the moment domain but his algorithm contains a time-consuming search in the parametric space and is sensitive to overestimation of the Gaussian variance. The APEX method [3] estimated the blur variance by fitting the image spectrum in the Fourier domain. There exist also several local methods that estimate the blur size by

investigating the response on a point source or on an ideal edge [4], [5]. A common weakness of these methods is their sensitivity to noise and the necessity of the prior knowledge where an ideal point or edge is located. Xue and Blu [6] proposed to estimate the blur variance by minimizing a proper functional and then to apply a non-blind Wiener filtering. As in the previous cases, the method is sensitive to the variance overestimation and relatively time-consuming.

The third and the most promising approach is based on the idea that for blur-insensitive recognition we do not need to restore the query image. We only need to have its representation (possibly low-dimensional and lossy) which is robust w.r.t. Gaussian blur. We are looking for a blur-invariant image descriptor  $I$ , which is a functional defined on the space of all images, such that

$$I(f) = I(f * h) \tag{2}$$

for any Gaussian kernel  $h$ . The existence of such Gaussian blur invariants is theoretically possible thanks to the fact that the Gaussian convolution is closed under the composition.<sup>1</sup> The closure property is an essential necessary condition. Imagine a set  $S$  of functions (convolution kernels) which would not be closed under convolution. Then  $I(f) = I(f * h_1) = I(f * h_1 * h_2)$  for arbitrary  $h_1, h_2 \in S$  but obviously  $(h_1 * h_2)$  may lie outside  $S$ . So, the functional  $I$  must be invariant to a convolution with a broader set of kernels. Such set is called *convolution closure* of  $S$  and we denote it as  $C(S)$ . If  $S \neq C(S)$ , then looking for the specific blur invariants w.r.t.  $S$  does not make sense. All such invariants must be at the same time invariant w.r.t.  $C(S)$ .

The idea of designing blur invariant functionals appeared about 20 years ago in the papers by Flusser *et al.* [7] and Flusser and Suk [8]. They proposed a system of blur invariants which are recursive functions of standard (geometric) moments of the image and proved their invariance under a convolution with arbitrary *centrosymmetric* kernel. These invariants, along with the centrosymmetry assumption, have been adopted by numerous researchers. They have become very popular image descriptors and have found a number of applications, namely in matching and registration of satellite and aerial images [8]–[12], in medical imaging [13]–[15], in normalizing blurred images into canonical forms [16], [17], in blurred digit and character recognition [18], in robot control [19], in image forgery detection [20], [21], in traffic sign recognition [22], [23], in fish shape-based classification [24], in wood industry [25], [26], and in cell recognition [27].

Several authors have further developed the theory of blur invariants. Combined invariants to convolution and to rotation were introduced by Flusser and Zitová [28], who also reported their successful usage in satellite image registration [29] and in camera motion estimation [30]. Combined invariants

<sup>1</sup>The set of all Gaussian functions with the binary operation convolution is a commutative monoid, i.e. a semigroup with a unit element. The closure property holds also for point-wise multiplication, so the Gaussians form a commutative ring. This assertion is valid for the set of normalized as well as unnormalized Gaussians. The Gaussian family is not the only parametric family of functions with the closure property to convolution; we recall  $\alpha$ -stable distributions known in statistics.

both to convolution and affine transform was published by Zhang *et al.* [17] and Suk and Flusser [31]. Their use for aircraft silhouette recognition [32], for sign language recognition [33], for the classification of winged insect [34] and for robust digital watermarking [35] was reported.

Some researchers attempted derivation of blur invariants which are functions of orthogonal moments rather than of the geometric moments. Legendre moments [36]–[39], Zernike moments [40]–[42], and Chebyshev moments [43] were employed for this purpose. Zuo *et al.* [44] even combined moment blur invariants and SIFT features [45] into a single vector with weighted components but without a convincing improvement. However, as was proved by Kautsky and Flusser [46], moment invariants in any two different polynomial bases are mutually dependent and theoretically equivalent.

Some other authors constructed the blur invariants in Fourier domain. Ojansivu and Heikkilä [47], [48] and Tang *et al.* [49] used blur-invariant properties of Fourier transform phase for image registration and matching. Their idea was later significantly generalized by Pedone *et al.* [50], [51]. Popular method of the *Local phase quantization* (LPQ) [52]–[55] also belongs to this group.

In almost all papers mentioned above, the invariance property was considered—exactly as in the original paper [8]—only to centrosymmetric PSF's. Few authors were apparently aware of this limitation which decreases the discrimination power and tried to construct invariants to more specific blurs. Flusser *et al.* derived invariants to motion blur [56], to axially symmetric blur in case of two axes [57], to circularly symmetric blur [58], and to arbitrary  $N$ -fold symmetric blur [59].

All the above methods do not use the parametric form of the PSF at all. They can be applied to Gaussian blur as well, because the Gaussian kernel is a special case of symmetric kernels. However, these methods cannot in principle reach the maximum possible discrimination power. To understand the discrimination power of the blur-invariant methods, we have to analyze the null-space of the respective invariants. The null-space is always formed by the functions with the same symmetry as the kernel symmetry the method is invariant to. To see that, we may imagine that the object is a blur kernel applied on the delta function. This means, invariants to centrosymmetric blur cannot discriminate among all centrosymmetric objects, invariants to circularly symmetric blur are not able to discriminate the circularly symmetric objects, etc. For instance the circle and the ring blurred by a Gaussian cannot be distinguished by invariants to centrosymmetric and circularly symmetric kernels but can be distinguished by invariants to Gaussian blur. For an optimal discriminability we need specific invariants exactly w.r.t. the blur which is present in the image. Unfortunately, the Gaussian blur invariants cannot be easily obtained as a special case of the earlier methods (even if the idea of projection operators we employ in this paper is similar to that one we proposed in [59]).

Only few attempts to derive invariants (2) w.r.t. Gaussian blur have been reported so far. Most of them are heuristics lacking a deeper mathematical analysis. Liu and Zhang [60] realized that the complex moments of the image, one index of

which is zero, are invariant to Gaussian blur. Xiao *et al.* [61] seemingly derived invariants to Gaussian blur but he did not employ the parametric Gaussian form explicitly. He only used the circular symmetry property which led to an incomplete invariant system. Gopalan *et al.* [62] derived another invariant set without assuming the knowledge of the parametric shape of the kernel but imposed a limitation of its support size. Flusser *et al.* mentioned an idea of Gaussian blur invariants in [63] without presenting the details and without testing their applicability.

An interesting approach, one of very few which have been proposed specifically for Gaussian blur and which works with a parametric form of the PSF, was proposed by Zhang *et al.* [64], [65]. They derived a blur-invariant distance measure  $d$  between two images which fulfills the condition

$$d(f_1, f_2) = d(f_1 * h, f_2) \quad (3)$$

for any Gaussian kernel  $h$ . Although the blur invariants are not explicitly defined, the invariant distance measure (3) can be used for object classification in a similar manner. The authors reported its good performance. The paper [65] published in this Transactions motivated us to perform a detailed study of their method, to analyze its pros and cons, and to propose a different approach based on invariants of the type (2) which outperforms the Zhang's method in several aspects.

The paper is organized as follows. Section II recalls the Zhang's method [65]. The new invariants based on projection operators are introduced in Section III. Section IV presents an experimental comparison of these two competing approaches along with a comparison to two general-purpose methods—cross correlation and LPQ.

## II. RECALLING THE ZHANG'S METHOD

The main idea of the method proposed in [65] is simple and elegant, even if some steps are hidden behind relatively complicated mathematical formalism which employs Riemannian manifolds. Here we briefly summarize the Zhang's method in a more transparent way.

The blur model used in [65] is supposed to be as in Eq. (1), where  $h$  is assumed to be a 2D circularly symmetric centralized Gaussian function  $G_\sigma(x, y)$  which is defined as

$$G_\sigma(x, y) = G_\sigma(x)G_\sigma(y), \quad (4)$$

where  $\sigma > 0$  and  $G_\sigma(x), G_\sigma(y)$  are 1D Gaussian functions of a traditional shape<sup>2</sup>

$$G_\sigma(x) = \frac{1}{\sqrt{2\pi}\sigma} e^{-\frac{x^2}{2\sigma^2}}$$

and of the same variance  $\sigma^2$ .

Let  $f_1, f_2$  be two images to be compared (their content as well as their blur level are generally different). First, the blur level of each of them is estimated by a proper blur measure. The authors used the integral of the image Laplacian but in principle any of the popular blur measures reviewed in [66] can be employed in this step. Both images are then brought

<sup>2</sup>Let us extend this definition by setting  $G_0(x) = \delta(x)$ .

to the same level of blurring which is chosen as the blur level of the more blurred image. This means that the (assumably) sharper image is blurred by a Gaussian kernel of a proper size to reach the same level of blur as the other image. This step should ensure that the distance measure becomes independent of the image blurring. Then the distance  $d(f_1, f_2)$  is defined as a geodesic distance on the surface of the ellipsoid which contains the images of the same blur level. This distance is calculated by means of an iterative “path straightening” algorithm. The only difference from a pure  $L_2$  norm is that the distance is measured along a curve on the ellipsoid surface but still it is based on a pixel-wise comparison of the images. It should be noted that in the earlier paper by the same authors [64], a simpler weighted  $L_2$  distance was used instead.

### III. GAUSSIAN BLUR INVARIANTS BASED ON PROJECTION OPERATORS

In this section we present an approach based on the *invariant descriptors* of the type (2). The basic conceptual difference from the Zhang’s method is that these invariants are defined for a single image, while the Zhang’s distance always requires a pair of images. So, we can calculate the invariant representations of the database objects/templates only once and store them in the database along with the object images. It leads to much faster recognition, as will be demonstrated practically in Section IV, and also yields a possibility of broader generalization.

The invariants are derived by means of projection operators in Fourier domain, as we will see in Theorem 1. For practical application, these complete invariants are replaced with equivalent image domain invariants, which are based on image moments. Derivation of both is the subject of the rest of this section.

#### A. Projection Operator in 1D

The new invariants are based on the projection of the image onto a space of unnormalized Gaussian functions, which preserves the image moments of the zeroth, the first, and the second orders. The separability of a 2D Gaussian function allows us to create a 1D theory (which is more transparent and easy to explain) first and then to generalize it to the 2D (or even  $N$ -D) case.

Let us consider a 1D “image”  $f$ ,  $f(x) \geq 0$ , with a finite non-zero integral and finite central moments of all orders. The projection operator  $P_G$  is defined as

$$P_G(f)(x) = m_0 G_s(x) \equiv \frac{m_0}{\sqrt{2\pi}s} e^{-\frac{x^2}{2s^2}}, \quad (5)$$

where

$$s^2 = m_2/m_0$$

and

$$m_p = \int (x - c)^p f(x) dx \quad (6)$$

is the  $p$ -th central moment of  $f$  (with  $c$  being the centroid of  $f$ ). Hence,  $P_G$  assigns each  $f$  to a centralized Gaussian

multiplied by  $m_0$  such that the central moments up to the second order of  $f$  and  $P_G(f)$  are equal. In other words,  $P_G(f)$  is the “closest” unnormalized Gaussian to  $f$  in terms of the first three moment values. In this sense,  $P_G$  can be considered a projector onto the set of unnormalized Gaussian functions.<sup>3</sup>

The operator  $P_G$  exhibits several interesting properties.

- Operator  $P_G$  is idempotent, i.e.  $P_G(P_G(f)) = P_G(f)$ .
- Operator  $P_G$  is multiplicative, i.e.  $P_G(af) = aP_G(f)$  for any constant  $a > 0$ .
- If  $f$  is an (unnormalized) Gaussian, then  $P_G(f) = f$  and vice versa.
- Any function  $f$  can be expressed as  $f = P_G(f) + f_n$ , where  $f_n$  can be considered a “non-Gaussian” part of  $f$ .
- The equality  $P_G(f_1) = P_G(f_2)$  defines an equivalence relation on the image space. The classes of equivalence are formed by the functions of the same zeroth and second central moments.

An important property of  $P_G$ , which will be later used for construction of the invariants, is its relationship to a convolution with a Gaussian kernel. It holds, for any  $f$  and  $\sigma$ ,

$$P_G(f * G_\sigma) = P_G(f) * G_\sigma. \quad (7)$$

To see this, we have to establish the relation between the second-order moments  $m_2^{(g)}$  on one hand and  $m_2^{(f)}$ ,  $m_2^{(h)}$  on the other hand. We recall (see [63] for details) that in general, for arbitrary  $f, h$ , and  $p$ , the moments are transformed under a convolution as

$$m_p^{(g)} = \sum_{k=0}^p \binom{p}{k} m_k^{(h)} m_{p-k}^{(f)}. \quad (8)$$

If  $h(x) = G_\sigma(x)$ , its moments are

$$m_k^{(h)} = \sigma^k (k-1)!! \quad (9)$$

for any even  $k$ . The symbol  $k!!$  means a double factorial,  $k!! = 1 \cdot 3 \cdot 5 \cdots k$  for odd  $k$ , and by definition  $(-1)!! = 0!! = 1$ . For any odd  $k$  the moment  $m_k^{(h)} = 0$  due to the symmetry of the Gaussian function. Hence, (8) obtains the form

$$m_p^{(g)} = \sum_{\substack{k=0 \\ k \text{ even}}}^p \binom{p}{k} \sigma^k (k-1)!! \cdot m_{p-k}^{(f)}. \quad (10)$$

In particular,

$$m_0^{(g)} = m_0^{(f)}$$

and

$$m_2^{(g)} = m_2^{(f)} + \sigma^2 m_0^{(f)}.$$

Now we can see that

$$P_G(f * G_\sigma)(x) = m_0 G_{\sqrt{(s^2 + \sigma^2)}}(x) = (P_G(f) * G_\sigma)(x) \quad (11)$$

(the latter equality follows from the fact that the convolution of two Gaussians is again a Gaussian with the variance being the sum of the input variances).

<sup>3</sup>However, it is not a projector in the common meaning, since it is not a linear operator and the Gaussians do not form a vector space.

### B. 1D Gaussian Blur Invariants in the Fourier Domain

Now we can formulate the central Theorem of this paper.

*Theorem 1:* Let  $f$  be an image function. Then

$$I_G(f)(u) = \frac{\mathcal{F}(f)(u)}{\mathcal{F}(P_G(f))(u)}$$

is an invariant to Gaussian blur, i.e.  $I_G(f) = I_G(f * G_\sigma)$  for any blur parameter  $\sigma$ .

The proof follows immediately from Eq (7). Note that  $I_G$  is invariant also to the contrast stretching,  $I_G(f) = I_G(af)$ .

What is the meaning of these invariants? The frequency domain provides us with a good insight.  $I_G(f)$  is a ratio of two Fourier transforms which may be interpreted as a deconvolution. Having an image  $f$ , we seemingly “deconvolve” it by the kernel  $P_G(f)$ , which is the largest possible Gaussian kernel (larger kernels cannot exist because de-blurring always monotonically decreases  $m_2$ , reaching the limit at  $m_2^{(\mathcal{F}^{-1}(I_G(f)))} = 0$ ). We call the result of this seeming deconvolution the *primordial image*

$$f_r = \mathcal{F}^{-1}(I_G(f)).$$

Hence,  $I_G(f)$  can be viewed as its Fourier transform, although  $f_r$  is not an image in a common sense because the existence of  $\mathcal{F}^{-1}(I_G(f))$  is not generally guaranteed and even if  $f_r$  exists, it may contain negative values.

$I_G(f)$  can be viewed as a kind of normalization of  $f$  w.r.t. Gaussian blurring of unknown extent. The primordial image plays the role of a canonical form of  $f$ , which actually is its “maximally deconvolved” non-Gaussian part. We can see a conceptual difference from the Zhang’s approach [65]. To make two images comparable, Zhang blurs them to the same level of blur, which is given by the more blurred image in the pair. We (seemingly) deblur each image separately because the canonical form is independent of the other images.

The equality  $I_G(f_1) = I_G(f_2)$  decomposes the image space into classes of equivalence. Fortunately, this decomposition is exactly the same as that one induced by the following relation: two functions  $f_1$  and  $f_2$  are equivalent if and only if there exist  $a > 0$  and  $\sigma \geq 0$  such that  $f_1 = f_2 * aG_\sigma$  or  $f_2 = f_1 * aG_\sigma$ . To prove this, let us first realize that if  $I_G(f_1) = I_G(f_2)$  then obviously

$$\mathcal{F}(f_1)(u)\mathcal{F}(P_G(f_2))(u) = \mathcal{F}(f_2)(u)\mathcal{F}(P_G(f_1))(u),$$

which in the image domain means

$$f_1 * P_G(f_2) = f_2 * P_G(f_1).$$

Both  $P_G(f_i)$  are (unnormalized) Gaussians. Let us denote their standard deviations as  $\sigma_1$  and  $\sigma_2$ , respectively, so we have  $P_G(f_i) = a_i G_{\sigma_i}$ . Let  $\sigma_1 \geq \sigma_2$ . We define  $\sigma^2 = \sigma_1^2 - \sigma_2^2$  and  $a = a_1/a_2$ . Since the convolution of any two Gaussians is again a Gaussian the variance of which is the sum of two input variances, we have

$$aG_\sigma * a_2G_{\sigma_2} = a_1G_{\sigma_1}.$$

From this we immediately obtain

$$f_1 = f_2 * aG_\sigma$$

which completes the proof.

This is an important observation, saying that  $I_G(f)$  is a *complete* description of  $f$  up to a convolution with a Gaussian and a multiplicative contrast change. In other words,  $I_G(f)$  defines an *orbit* – a set of images equivalent with  $f$ . Thanks to the completeness,  $I_G$  discriminates between the images from different orbits but obviously cannot discriminate inside an orbit. In particular,  $I_G$  cannot discriminate between two Gaussians since all Gaussians lie on the orbit the root of which is the delta function.

### C. 1D Gaussian Blur Invariants in the Image Domain

In principle, we can use directly  $I_G(f)$  as the invariant feature vector of the same size as  $f$  but working in the Fourier domain brings two practical difficulties. Since  $I_G(f)$  is a ratio, we possibly divide by very small numbers which requires an appropriate numerical treatment. Moreover, high frequencies of  $I_G(f)$  use to be sensitive to noise. This can be overcome by suppressing them by a low-pass filter, but this procedure introduces a user-defined parameter (the cut-off frequency) which should be set up with respect to the particular noise level. That is why in most cases we prefer to work directly in the image domain, where invariants equivalent to  $I_G(f)$  can be constructed.

To get the link between the Fourier and image domains, we use a Taylor expansion of the harmonic functions and its term-wise integration

$$\mathcal{F}(f)(u) \equiv \int_{-\infty}^{\infty} f(x) \cdot e^{-2\pi i u x} dx = \sum_{k=0}^{\infty} \frac{(-2\pi i)^k}{k!} m_k u^k. \quad (12)$$

The above formula tells us that the moments of the image are Taylor coefficients (up to a constant factor) of its Fourier transform. Taylor expansion of  $\mathcal{F}(P_G(f))$  yields

$$\mathcal{F}(P_G(f))(u) = m_0 \sum_{k=0}^{\infty} (2k-1)!! \frac{(-2\pi i)^{2k}}{(2k)!} \left(\frac{m_2}{m_0}\right)^k u^{2k} \quad (13)$$

(we recall  $\mathcal{F}(P_G(f))$  is a Gaussian).

We can see  $I_G(f)$  is a ratio of two absolutely convergent power series, so  $I_G(f)$  itself can be expressed as an absolutely convergent power series of the form

$$I_G(f)(u) = \sum_{k=0}^{\infty} \frac{(-2\pi i)^k}{k!} a_k u^k$$

where  $a_k$  are the moments of the primordial image. Substituting the above three power series into the definition of  $I_G(f)$  and considering that

$$(2k-1)!! = \frac{(2k)!}{2^k \cdot k!}$$

we have

$$\sum_{k=0}^{\infty} \frac{(-2\pi i)^k}{k!} m_k u^k = m_0 \sum_{k=0}^{\infty} \frac{(-2\pi i)^k}{k!} \left(\frac{m_2}{m_0}\right)^k u^{2k} \cdot \sum_{k=0}^{\infty} \frac{(-2\pi i)^k}{k!} a_k u^k.$$

Comparing the terms with the same power of  $u$  we obtain, after some algebraic manipulation, the recursive expression for each  $a_p$

$$a_p = \frac{m_p}{m_0} - \sum_{\substack{k=2 \\ k \text{ even}}}^p (k-1)!! \cdot \binom{p}{k} \left(\frac{m_2}{m_0}\right)^{k/2} a_{p-k}. \quad (14)$$

Since the primordial image itself (more precisely, its Fourier transform) was proven to be blur invariant, each its moment must be also a blur invariant. If we restrict ourselves to a brightness-preserving blurring, then  $m_0$  itself is an invariant and we obtain from (14) the simplified final form of Gaussian blur invariants

$$B(p) \equiv m_0 a_p = m_p - \sum_{\substack{k=2 \\ k \text{ even}}}^p (k-1)!! \cdot \binom{p}{k} \left(\frac{m_2}{m_0}\right)^{k/2} B(p-k), \quad (15)$$

which can be equivalently expressed in a non-recursive form

$$B(p) = \sum_{\substack{k=0 \\ k \text{ even}}}^p (k-1)!! \cdot \binom{p}{k} \left(-\frac{m_2}{m_0}\right)^{k/2} m_{p-k}. \quad (16)$$

For the proof of the equivalence of (15) and (16) see Appendix A.

As we already said,  $B(p)$  is actually a  $p$ -th moment of the primordial image of  $f$ . Regardless of  $f$ ,  $B(1) = 0$  because we work with central moments<sup>4</sup>  $m_p$ . It always holds  $B(2) = 0$  because the second-order moment was used to eliminate the unknown blur parameter  $\sigma$ . Hence,  $B(1)$  and  $B(2)$  should not be used in the feature vector since they do not carry any information.

Using the image-domain invariants (15) instead of the Fourier domain ones provides higher robustness to noise and is also faster. In practice, we do not need a complete representation of the images in question. Usually a few invariants provide a sufficient discrimination power, so we use the  $B(p)$ 's up to the certain order  $Q$  only. This  $Q$  is a user-defined parameter the determination of which should be based on a discrimination analysis of the database images. The choice of  $Q$  is always a compromise between the discriminative power and the complexity of the method.

#### D. Gaussian Blur Invariants in $N$ Dimensions

Let us assume the image domain is a subset of  $R^N$ . The centralized  $N$ -D Gaussian function has the form

$$G_{\Sigma}(\mathbf{x}) = \frac{1}{\sqrt{(2\pi)^N |\Sigma|}} \exp\left(-\frac{1}{2} \mathbf{x}^T \Sigma^{-1} \mathbf{x}\right), \quad (17)$$

where  $\mathbf{x} \equiv (x_1, \dots, x_N)^T$  and  $\Sigma$  is the covariance matrix which determines the shape of the Gaussian. Provided that

<sup>4</sup>This theory is valid also when using standard non-centralized moments. Then generally  $B(1) \neq 0$  but working with central moments is advantageous since it assures the shift invariance.



Fig. 2. The original image  $f$  (a) and its projection  $P_G(f)$  (b).

$N = 2$  and that the covariance matrix of the blur kernel is diagonal, we define the projection operator as

$$P_G(f)(\mathbf{x}) = m_{00} G_S(\mathbf{x}), \quad (18)$$

where

$$S = \text{diag}(m_{20}/m_{00}, m_{02}/m_{00}).$$

The definition of the central geometric moments  $m_{pq}$  in two dimensions is analogous to that in one dimension

$$m_{pq} = \int \int (x_1 - c_1)^p (x_2 - c_2)^q f(x_1, x_2) dx_1 dx_2. \quad (19)$$

A visual example of the projection operator is shown in Fig. 2. Similarly to the 1D case (see Theorem 1), the ratio

$$I_G(f)(\mathbf{u}) = \frac{\mathcal{F}(f)(\mathbf{u})}{\mathcal{F}(P_G(f))(\mathbf{u})}$$

is a Gaussian blur invariant. After applying the Taylor expansion, we end up with the following moment invariants analogous to (15)

$$B(p, q) = m_{pq} - \sum_{\substack{k+j=2 \\ k, j \text{ even}}}^{p, q} (k-1)!! \cdot (j-1)!! \cdot \binom{p}{k} \binom{q}{j} \times \left(\frac{m_{20}}{m_{00}}\right)^{k/2} \left(\frac{m_{02}}{m_{00}}\right)^{j/2} B(p-k, q-j) \quad (20)$$

which can be rewritten into a non-recursive form analogous to (16) as

$$B(p, q) = \sum_{\substack{k, j=0 \\ k, j \text{ even}}}^{p, q} (k-1)!! \cdot (j-1)!! \cdot \binom{p}{k} \binom{q}{j} \times \left(-\frac{m_{20}}{m_{00}}\right)^{k/2} \left(-\frac{m_{02}}{m_{00}}\right)^{j/2} m_{p-k, q-j}. \quad (21)$$

For the general case of  $N > 2$  see Appendix B.

Note that unlike the Zhang's method, we are not limited to circularly symmetric Gaussian blur kernels but we allow different extent of blur in  $x_1$  and  $x_2$  directions.<sup>5</sup> This may be useful when the horizontal and vertical resolutions of the sensor differ one another. Again, certain invariants are trivial:  $B(1, 0) = B(0, 1) = 0$  due to the centralization,  $B(2, 0) = B(0, 2) = 0$  due to the parameter elimination.<sup>6</sup>

<sup>5</sup>The Zhang's method could very likely be also generalized to non-isotropic blurs but on the expense of additional time.

<sup>6</sup>If the blur kernel is circularly symmetric, there is only one parameter to be eliminated and we obtain an additional independent invariant  $m_{20} - m_{02}$ .

### E. Translational, Scaling, and Rotational Invariance

Invariance w.r.t. to image translation, scaling and rotation (TSR) is one of the basic requirements we impose on almost any features. If the images are not captured in a fully controlled environment, we always face certain unavoidable unwanted translation/scaling/rotation of the scene.

The Zhang's method is not invariant to translation, scaling, and rotation. This issue was not discussed at all in [65] and the experiments were presented on perfectly registered images only. We believe the Zhang's method could be adapted to be translational invariant but we cannot see any possible extension to scaling and rotation invariance except a time-expensive brute force search.

The invariants  $B(p, q)$ , introduced in the previous section, are inherently invariant to translation, because they are composed of the central moments of the image. Scaling invariance can be achieved by using the scale-normalized moments instead of the standard moments. This is a commonly used approach in the moment theory (see [63] for details), which is in this case equivalent to dividing each  $B(p, q)$  by  $m_{00}^{(p+q+2)/2}$ .

Since the standard moments change under rotation in a complicated way, the rotation invariance of  $B(p, q)$  cannot be achieved readily (let us speak about the 2D case only because handling the rotation in higher dimensions requires special mathematical tools and it is of less practical importance). We will adopt the trick discovered by Flusser [67], who used it for construction of rotation moment invariants (with no relationship to blurring).

First of all, we have to use other moments than the geometric ones, which change under rotation in a simple way. There exist a class of such moments (see [63] for a survey) called *radial moments*. Their common feature is that their 2D basis functions are products of 1D radial polynomials and angular harmonic functions. They use to be complex valued and under the image rotation only their phase is changed (the reader can recognize a clear analogy with the Fourier Shift Theorem). Here we employ so-called *complex moments*

$$c_{pq} = \int_{-\infty}^{\infty} \int_{-\infty}^{\infty} (x + iy)^p (x - iy)^q f(x, y) dx dy \quad (22)$$

that are linked to the previously used geometric moments as

$$c_{pq} = \sum_{k=0}^p \sum_{j=0}^q \binom{p}{k} \binom{q}{j} (-1)^{q-j} \cdot i^{p+q-k-j} \cdot m_{k+j, p+q-k-j} \quad (23)$$

and inversely as

$$m_{pq} = \frac{1}{2^{p+q} i^q} \sum_{k=0}^p \sum_{j=0}^q \binom{p}{k} \binom{q}{j} (-1)^{q-j} \cdot c_{k+j, p+q-k-j}. \quad (24)$$

Note that  $c_{pq} = c_{qp}^*$ , so only the moments with  $p \geq q$  are independent and meaningful to consider. After a transformation into polar coordinates  $(r, \theta)$ , the complex moments obtain

the form

$$c_{pq} = \int_0^{\infty} \int_0^{2\pi} r^{p+q+1} e^{i(p-q)\theta} f(r, \theta) d\theta dr. \quad (25)$$

From the last equation we can see that after a coordinate rotation by angle  $\alpha$  the complex moment is changed as

$$c'_{pq} = e^{-i(p-q)\alpha} \cdot c_{pq}. \quad (26)$$

The complex moments of the blurred image (1) are in general

$$c_{pq}^{(g)} = \sum_{k=0}^p \sum_{j=0}^q \binom{p}{k} \binom{q}{j} c_{kj}^{(h)} c_{p-k, q-j}^{(f)}. \quad (27)$$

If the blur kernel  $h$  is a circularly symmetric Gaussian (4) then we have for its moments

$$c_{pq}^{(h)} = \begin{cases} (2\sigma^2)^p p! & p = q \\ 0 & p \neq q \end{cases}$$

and Eq. (27) becomes

$$c_{pq}^{(g)} = \sum_{j=0}^q \binom{p}{j} \binom{q}{j} j! (2\sigma^2)^j c_{p-j, q-j}^{(f)}, \quad (28)$$

assuming that  $p \geq q$ .

Now we use the complex moments to derive invariants w.r.t. Gaussian blur in a similar way as the geometric moments were used earlier. Similarly to Eq. (5), we define the projection operator as

$$P_G(f)(x, y) = c_{00} G_s(x, y) \equiv \frac{c_{00}}{2\pi s^2} e^{-\frac{x^2+y^2}{2s^2}}, \quad (29)$$

where

$$s^2 = c_{11}/(2c_{00}).$$

$P_G(f)$  has the same  $c_{00}$  and  $c_{11}$  as  $f$  (and of course  $c_{10} = 0$  when working in the centralized coordinates). The other moments of  $P_G(f)$  and  $f$  are generally different from one another. The following relation shows that the complex moments are "almost" the Taylor coefficients of the Fourier transform of  $f$ . Let us make a substitution  $U = u + v$  and  $V = i(u - v)$ . Then

$$\begin{aligned} \mathcal{F}(f)(U, V) &\equiv \int_{-\infty}^{\infty} \int_{-\infty}^{\infty} e^{-2\pi i(Ux+Vy)} f(x, y) dx dy \\ &= \sum_{j=0}^{\infty} \sum_{k=0}^{\infty} \frac{(-2\pi i)^{j+k}}{j!k!} c_{jk} u^j v^k. \end{aligned} \quad (30)$$

Using the same substitution, we define the blur invariant in Fourier domain analogously to Theorem 1 as

$$I_G(f)(U, V) = \frac{\mathcal{F}(f)(U, V)}{\mathcal{F}(P_G(f))(U, V)}.$$

Taylor expansion of the denominator is

$$\mathcal{F}(P_G(f))(U, V) = c_{00} \sum_{k=0}^{\infty} \frac{(-4\pi^2)^k}{k!} \left( \frac{c_{11}}{c_{00}} \right)^k u^k v^k.$$

Using the Taylor expansion of all three factors by means of their complex moments and comparing the coefficients of the same powers, we obtain the blur invariants in the image domain

$$\begin{aligned}
 K(p, q) &= c_{pq} - \sum_{k=1}^q k! \binom{p}{k} \binom{q}{k} \left(\frac{c_{11}}{c_{00}}\right)^k K(p-k, q-k) \\
 &= \sum_{k=0}^q k! \binom{p}{k} \binom{q}{k} \left(-\frac{c_{11}}{c_{00}}\right)^k c_{p-k, q-k}. \quad (31)
 \end{aligned}$$

Note that  $K(q, p) = K(p, q)^*$ ,  $K(1, 0) = 0$  when working in the centralized coordinates, and  $K(1, 1) = 0$  due to the parameter elimination.

The invariants  $K(p, q)$  are formally similar to the  $B(p, q)$ 's (only the moment type was changed). They are actually different but thanks to the link between the geometric and complex moments (23, 24) they generate the same invariant subspace. The principle difference between them (and the reason why we employed the complex moments in this section) is that the  $K(p, q)$ 's are easy to handle under an image rotation. They change in the same way as the complex moments themselves, i.e.

$$K'(p, q) = e^{-i(p-q)\alpha} \cdot K(p, q). \quad (32)$$

The simplest way to achieve the rotation invariance is to take the magnitudes  $|K(p, q)|$  which provide combined invariants but create only an incomplete system. A more sophisticated method is based on the phase cancellation by multiplication of proper invariants, which leads for instance to the invariants<sup>7</sup>

$$K(p, q)K(1, 2)^{p-q}.$$

Scale invariance of  $K(p, q)$ 's can be achieved by the same normalization as in the case of  $B(p, q)$ 's.

#### IV. EXPERIMENTS AND A COMPARISON TO THE ZHANG'S METHOD

The aim of this section is not only to demonstrate the performance of the proposed method but also to compare it to the method by Zhang *et al.* [65]. Comparison to the Zhang's method is highly relevant because both methods have been designed specifically for Gaussian-blurred images, both are theoretically invariant to blur and both should provide good recognition power. There have been proposed no other competitors of these properties in the literature. To make the comparison as fair as possible, we asked the authors of [65] for providing all necessary original codes. Then we implemented our method using the same version of Matlab (R2013a) and always run both on the same computer (Dell Notebook, VOSTRO 1510, Intel, Core2 Duo CPU, 4GB RAM, Windows 8, 32-bit) and on the same test images. Since the Zhang's method can compare only images of the same size, we kept this condition in all experiments.

In some experiments we included also two other method into the comparison – image cross-correlation and Local phase quantization (LPQ) [52]–[55]. The cross-correlation is of

<sup>7</sup>This set can be proven to be complete and independent provided that  $K(1, 2) \neq 0$ . Other choices are also possible and lead to equivalent invariants.

TABLE I

THE VALUES OF ZD AND ID IN THE CASE OF SIMULATED GAUSSIAN BLUR

$\sigma$	Filter size	ZD	ID
0	1	0	0
1	9	0.112	2e-19
2	17	0.005	1e-19
3	25	0.009	3e-19
4	33	0.012	4e-19
5	41	0.014	6e-19
6	49	0.016	2e-19
7	57	0.017	2e-19

course not blur invariant, so the comparison with it shows what is the actual benefit of the blur invariance property. LPQ is a representative of methods acting in the Fourier domain. LPQ is invariant to general centrosymmetric blur, it does not employ the parametric form of the PSF at all. The main idea is that a centrosymmetric PSF does not change the phase of the Fourier transform in certain neighborhood of the origin. The Fourier transform is windowed and its phase in a close neighborhood of the origin is quantized and taken as a local descriptor. We originally used the LPQ code provided by the authors which we later improved to reach better performance. Some other method had been compared to the Zhang's distance (ZD) already in [65]. The reader can find there a comparison to standard Euclidean distance, the Gopalan method [62], and centrosymmetric blur invariants [8]. Since the ZD had been evaluated as the best performing method among these, we did not incorporate these comparative methods into our current tests.

The first set of the experiments only illustrates the properties of both methods, which already were proved theoretically. The core experiments can be found in the second set, where statistically significant comparison of the success rate and the time complexity is presented.

##### A. Blur Invariance Property

As we expected, both methods actually exhibit high invariance w.r.t. a "perfect" (i.e. computer-generated) Gaussian blur (see Table I). We changed the blur parameter  $\sigma$  from 0 to 7 and calculated both the Zhang's distance ZD and the Euclidean distance in the space of the invariants (31) between the blurred image and the original. We refer to the distance in the space of the invariants as the *invariant distance* ID. Both distances in this experiment are reasonably small although not zero. The non-zero values appear because the sampled Gaussian does not fulfil exactly the assumption. Since larger sampled Gaussians are more accurate, we observe that the error sometimes decreases as the blur size increases, although one might expect an opposite relation. For comparison, we also calculated the distances between several *different* originals, which is by two orders higher. The test images were of the size  $160 \times 160$  pixels (see Fig. 3 for an example).

##### B. Shift, Rotation, and Scaling Invariance

Here we experimentally verified the theoretical knowledge that our method provides the invariance w.r.t. these three elementary geometric transformations while the Zhang's method



Fig. 3. One of the original images ( $160 \times 160$  pixels) used in the tests.

TABLE II  
THE DISTANCE BETWEEN THE ORIGINAL AND ITS SHIFTED COPY

Shift (in pixels)	ZD	ID
0	0	0
5	435	2e-19
10	548	2e-19
15	607	0
20	630	3e-19
25	639	2e-20
30	644	2e-20
35	647	7e-20

TABLE III  
THE DISTANCE BETWEEN THE ORIGINAL AND ITS ROTATED COPY

Rotation angle [deg]	ZD	ID
0	0	0
10	389	7e-10
20	452	2e-9
30	462	9e-9
40	443	1e-8
50	416	1e-8
60	380	5e-9
70	339	2e-9
80	291	1e-10
90	230	1e-19

TABLE IV  
THE DISTANCE BETWEEN THE ORIGINAL AND ITS SCALED COPY

Scaling factor	ZD	ID
1	0	0
0.8	589	1e-6
0.6	716	1e-6
0.4	774	3e-6
0.2	829	1e-5

is sensitive to the particular image position, orientation and size. It is worth mentioning how sensitive the ZD is to the shift. As the shift approaches 5 pixels, the Zhang distance between the shifted images is comparable to the distance between two completely different images (see Table II). The same is true for the scaling and rotation, too. Even a small rotation/scaling harms the ZD substantially (see Table III and Table IV). The sensitivity to a shift is also a weakness of the LPQ method. The Fourier phase is changed when the image has been shifted, so the LPQ feature is changed as well. There exist rotation and scale invariant modifications of LPQ but no shift invariant version has been reported.

TABLE V  
THE DISTANCE BETWEEN THE ORIGINAL AND ITS CONTRAST-CHANGED COPY

Contrast factor	ZD	ID
1	0	0
0.9	90	5e-10
0.8	180	2e-10
0.7	270	2e-10
0.6	359	4e-10
0.5	449	0
0.4	538	2e-10
0.3	625	4e-9
0.2	708	2e-10
0.1	783	2e-10

### C. Invariance to Contrast Stretching

This easy test verified that the invariants, when normalized by  $m_{00}$ , are invariant also to a contrast stretching of the form  $g(x, y) = af(x, y)$ ,  $a > 0$ . The Zhang's method interprets low contrast as a blur due to lower values of the Laplacian and blurs the more contrast image before the distance is calculated. This leads to an inaccuracy of computation of the ZD, which of course depends on the parameter  $a$  (see Table V for illustration). However, this problem of the ZD can easily be resolved by normalizing the images to the same graylevel variance (which, on the other hand, would increase the time complexity).

### D. Robustness to Noise

Robustness to additive noise is an important requirement imposed on any features since in reality the noise is unavoidable. When taking a picture in low light, we use high ISO and/or long exposure. Both amplifies the background noise, which is present in any electronic system, such that the noise energy may be even higher than that of the signal. Particularly compact cameras and cell-phone cameras with small-size chips suffer from this kind of noise, along with an omnipresent thermal noise. Although the camera noise contains also a Poisson component, it is commonly modelled as a white Gaussian noise.

First, we added the noise of SNR from 50 dB to  $-5$  dB into the image (see Fig. 4 for some examples), and calculated both ID and ZD from the original. On each noise level, we run the experiment 10 times and the mean values are presented in Table VI. The invariant method is more robust because the moments are defined as integrals, which basically "averages" the noise and decreases its impact on the feature values. On the other hand, the Zhang distance is very sensitive. This is due to its first stage when the image blur level is estimated by measuring the energy in the high-pass band. The noise dominates the image on high frequencies and contributes a lot to this measure. Hence, the blurred image with heavy noise may often be considered "sharper" than the clear image and the method blurs it again to bring it (seemingly) to the same blur level.

We measured the robustness also on real noise. We took a series of photographs in low-light conditions to introduce an observable camera noise. Each of four scenes used here was

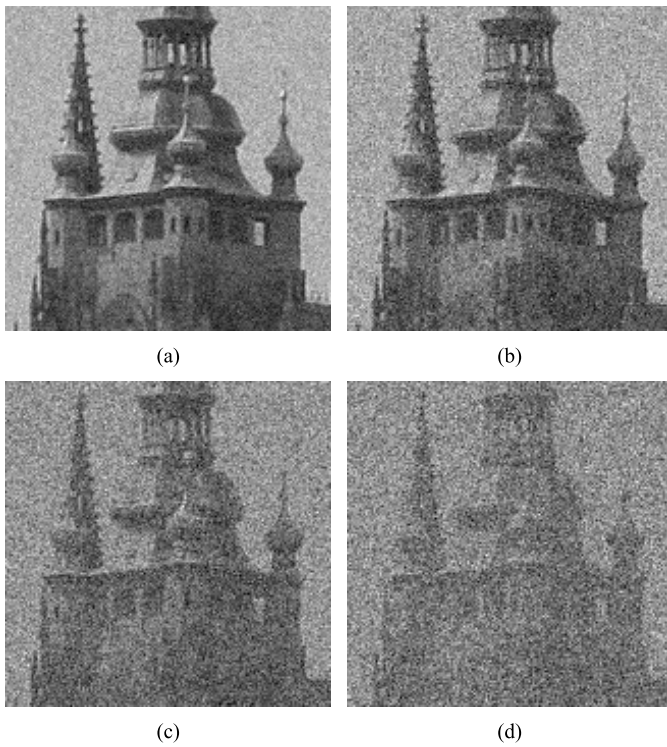


Fig. 4. Examples of the images with simulated noise used in the test. SNR = 10 dB (a), SNR = 5 dB (b), SNR = 0 dB (c), and SNR = -5 dB (d).

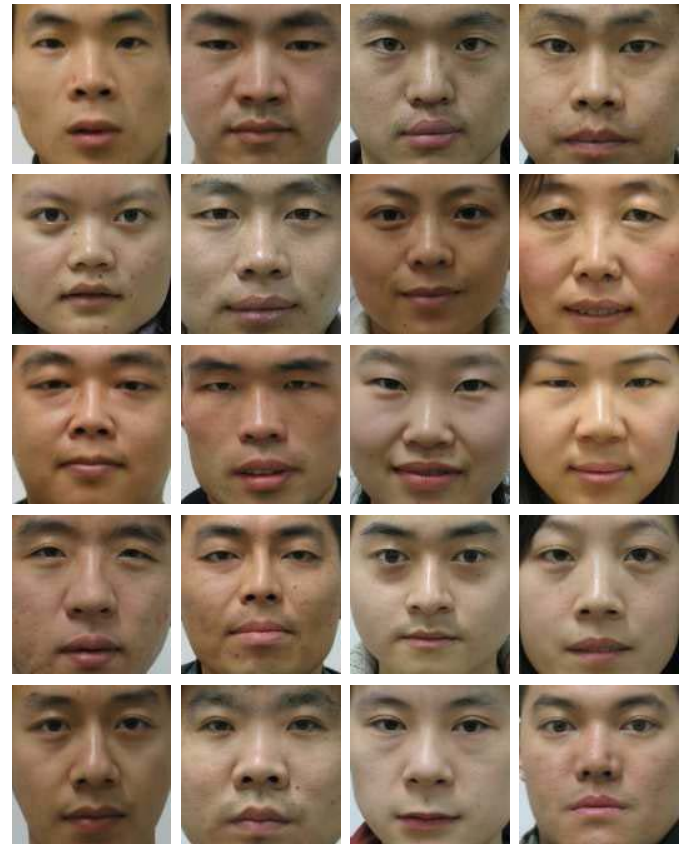


Fig. 5. Sample “clear” images of the challenging database. The database consists of very similar faces. Downloaded from the CASIA HFB dataset.

TABLE VI  
THE DISTANCE BETWEEN THE ORIGINAL AND ITS NOISY VERSION – SIMULATED NOISE

SNR [dB]	ZD	ID
50	1.1	1e-8
40	3.6	3e-8
30	11.0	1e-7
20	31.3	3e-7
10	71.0	1e-6
5	98.7	1e-6
0	135.9	9e-6
-5	193.0	3e-5

TABLE VII  
THE DISTANCE BETWEEN THE ORIGINAL AND ITS NOISY VERSION – REAL NOISE

Scene	ZD	ID
1	2.39	2e-6
2	2.07	2e-6
3	1.76	7e-7
4	1.35	4e-6

taken by a multi-shot sequence of 20 frames. The estimated SNR in each frame is about 30 dB. The “clear” image was obtained by a time-averaging of the noisy frames, since it was not possible to take it directly. Such an image is not actually noise-free but the noise is suppressed significantly. For each scene, we calculated both ID and ZD between the “clear” image and each noisy frame. The mean values for each scene are presented in Table VII. Considering that the ideal distance value should be always zero, these results are consistent with those obtained on simulated noise and confirm the better robustness of the ID.

### E. Image Recognition Against Public Databases

The main purpose of ZD and ID is to use them in recognition of Gaussian-blurred images w.r.t. a given database of clear images. As soon as the query image is provided, both ZD and ID look for exactly the same image (up to the blurring and the contrast change) in the database. This recognition should be reliable and fast enough. These methods do not tolerate other differences such as nonlinear deformations, object pose, facial expression, etc. They are inappropriate in the cases where such situation may occur. Since the “image classes” are defined by single representatives, the classification by minimum distance is applied most often.<sup>8</sup>

First of all, we used LIVE and CSIQ databases [68], [69], which were used already in [65]. To our best knowledge, these two databases are the only public datasets containing Gaussian-blurred images. The CSIQ database contains 30 clear images of common urban, animal and landscape scenes and five blurred instances of various extent of each of them. The LIVE database contains similar data but only some of the images are available along with their blurred versions. To reach higher statistical significance, we mixed both databases together. We resampled all images to 128 × 128 pixels, used 59 clear images as training samples and classify all 324 blurred images by ID, ZD and LPQ. The success rate of all three methods was 100%. This is because the training images

<sup>8</sup>This is, however, not a restriction imposed by ZD/ID themselves. If the training set contained more samples, we could apply *k*-NN or SVM classifiers.

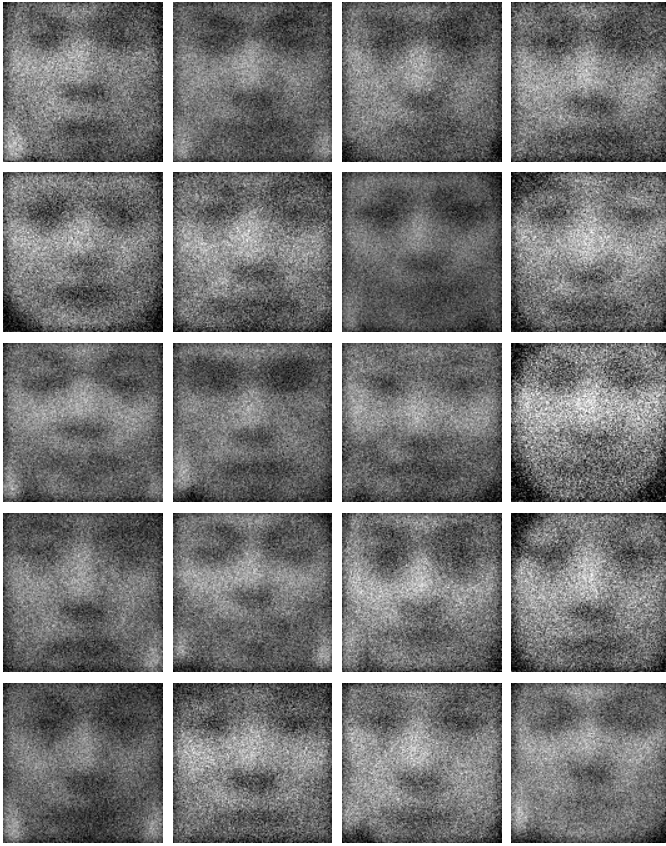


Fig. 6. Sample test images degraded by heavy blur and noise ( $\sigma = 5$  and SNR = 0 dB).

are visually clearly different and therefore the blur introduced into the query image does not cause serious problems. Concerning the time, ID was the fastest, LPQ was about ten times slower and ZD was more than 1000 times slower than ID.

For the second experiment we deliberately used a database which is composed of similar images, which are even difficult to distinguish visually. In such a case even a mild blur and noise might result in a number of misclassifications. Although the tested methods have not been developed as specialized face recognition methods, we used facial database for two reasons—it contains very similar images and blur is often present in face recognition applications. We selected 100 face images of 100 persons from the CASIA heterogeneous face biometrics (HFB) database [70], [71]. They are all frontal views with a neutral expression, without a head pose, and with the face being cropped (see Fig. 5). We successively took each image of the dataset, blurred it by a Gaussian blur, added a noise, and classified the image by the minimum distance rule against the database of the “clear” images (see Fig. 6 for the samples of the most degraded images). We did this for various amount of blur and noise and measured the success rate. For each blur and noise level we generated ten instances of the query image. Hence, we classified 36,000 images altogether.

The results of all three methods are summarized in a form of the “blur size – SNR” matrices in Table VIII. While for low amount of blur and noise all methods work very well, the performance of ZD drops as the image degradations increase (check the lower right part of the matrix). The performance

TABLE VIII  
RECOGNITION RATE (IN %) OF BLURRED AND NOISY  
FACES BY ZD, LPQ AND ID

SNR [dB]/ $\sigma$	0	1	2	3	4	5
Method	ZD					
60	100	100	100	100	100	100
40	100	100	100	100	100	100
20	100	100	100	100	97	74
10	100	100	100	82	48	30
5	100	100	100	74	41	26
0	100	100	98	60	35	21
Method	LPQ					
60	100	100	100	100	100	96
40	100	100	100	100	100	95.9
20	100	100	100	100	100	95.6
10	100	100	100	100	99.9	93.6
5	100	100	100	100	99.6	91.6
0	100	100	99.9	99.5	93	69.9
Method	ID					
60	100	100	100	100	100	100
40	100	100	100	100	100	100
20	100	100	100	100	100	100
10	100	100	100	100	100	100
5	100	100	100	100	99.9	99.8
0	100	96	95	95	94	94

of the LPQ is comparable to that of the ID except the last column corresponding to the largest blur ( $\sigma = 5$ ), where the ID performs much better.

The success rate of the ID is almost 100% in all cases except SNR = 0 dB, which is mainly due to the guaranteed invariance of the ID w.r.t. blur and good robustness to additive noise.

We also measured the time needed for recognition of one image (this time does not depend on the particular configuration of the blur and noise). The Zhang’s method requires 1500 seconds, the LPQ 0.22 second and the proposed method works in 0.05 second only. This difference in complexity is mainly caused by the fact that the invariant values as well as the LPQ descriptors of the database images are calculated only once and used repeatedly, while the Zhang’s distance is calculated “from scratch” for each pair. The LPQ feature is of a high dimension comparing to the invariants. When calculating ID, only the invariants up to the order 8 were used, while the LPQ feature in the basic version has the same size as the image itself. Since the features are supposed to be stored in the database for a repeated usage, this high dimensionality makes the LPQ method inefficient in terms of the memory usage. The LPQ features can be quantized and compressed into a histogram only which speeds up the recognition and improves the memory usage (we actually used this trick in our experiment), but the dimensionality is still at least by one order higher than the dimensionality of the blur invariants. On the other hand, thanks to its redundancy, the LPQ achieves relatively good recognition rates.

#### F. Matching of Blurred Templates - Simulated Blur

In this experiment we tested the performance in the template matching, which is a particular classification problem we often face in practice. Assuming that we have a large clear image of a scene and a blurred template, the task is to localize this template in the clear image. We again tested both ID and ZD.



Fig. 7. Explanation of the boundary effect. The inside pixels near the template boundary (white square) are affected by the pixels from the outside of the template if the scene is blurred. The extent of this effect depends on the blur size (black square).

For a comparison we included also the cross-correlation (CC) as a “gold standard” method which has been traditionally used in matching of non-blurred templates. Since the testing of each possible template location is very time consuming, we used all three methods in a hierarchical coarse-to-fine implementation. On the coarse level, we shifted the template by the step of 4 pixels in each direction. On the fine level, we searched a  $9 \times 9$  neighborhood of the “best” location found on the coarse level. Provided that the horizontal and vertical localization errors are independent and both have the same normal distribution, the absolute localization error has a Rayleigh distribution. We estimated the mean values and standard deviations of the localization error of all three methods, which illustrates the accuracy. Since these parameters might be influenced by few big errors, we also calculated the number of “correct hits”, which may serve as another (and probably more relevant) accuracy measure. We marked the position of the template found by the algorithm as a hit, if its localization error was less or equal to one pixel in each direction.

Note that in template matching, when the blurred templates have been extracted from a large scene, we always face a *boundary effect*. This means there is a strip along the template boundary where the convolution model is not valid (even if the blur has been introduced artificially) because the pixels laying outside the template also contribute to the intensity values inside this strip due to the blurring kernel (see Fig. 7). The boundary effect is the main source of errors in a noise-free case.

We took a clear image of the size  $256 \times 256$ , blurred it by a  $13 \times 13$  Gaussian of  $\sigma = 2$  and randomly selected 30 templates of the size  $32 \times 32$ . These templates were searched in the clear image. We used the invariants up to the order six. The results of the matching in terms of the accuracy and computational time are summarized in Table IX. We can see that the accuracy of both ID and ZD are excellent, so both methods are stable w.r.t. the boundary effect. The ZD yields even better localization error than ID because it uses a complete information about the template while the invariants work with highly compressed information. On the other hand, ID is more than 20 times faster than ZD. The CC was much faster than ID but its accuracy was very low because of the blurring. The time measurement for one template includes a complete “scan” of the scene including invariant and distance calculation for each tested position and search for the minimum distance. Overheads (reading of the images, generating blur kernel, blurring the image, template selection, etc.)

TABLE IX  
MATCHING OF BLURRED NOISE-FREE TEMPLATES

Method	Mean error	Std	Mean time [s]	Correct hits
CC	42.53	22.22	1.29	23
ZD	0.16	0.08	831.5	30
ID	0.39	0.20	34.6	30

TABLE X  
MATCHING OF BLURRED AND NOISY TEMPLATES

Method	Mean error	Std	Mean time [s]	Correct hits
CC	41.24	21.55	1.31	20
ZD	43.99	22.98	825.1	15
ID	0.90	0.47	33.1	28



Fig. 8. The test image “Fox”: (a) original, (b) blurred image, (c) blurred and noisy image, SNR = 10 dB.

are common for all methods and were not included into the measurement.

Then we repeated the same experiment with the same setting and with the same templates but we added a Gaussian white noise of SNR = 10 dB into the blurred image (see Fig. 8). As can be seen from Table X, the results changed dramatically. The ID still provides 28 correct hits and the mean error less than one, while the ZD was even worse than the CC. The explanation of the difference in robustness is the same as that given in Section IV.D. The time complexity is basically the same as in the first experiment.

We also studied the behavior of the invariants under variable blur and template size and on various noise levels. In all following experiments we used the invariants up to the order 6. First, we fixed the template size to  $32 \times 32$  while the Gaussian  $\sigma$  increased from 1 to 5 by a sampling step 0.5. In each parameter setting we matched 30 randomly chosen templates. This experiment was run five times and the means of the correct hits are shown in a graph in Fig. 9. Then we run the whole experiment again with the same templates corrupted by a noise of SNR = 0 dB. As one may expect, the results are much worse namely in case of small blur (see Fig. 9). In case of heavy blur, the main source of errors is a boundary effect and the influence of noise is not so significant.

In a complementary experiment, we fixed  $\sigma = 2$  and changed the SNR only. The means of the correct hits over 30 runs are shown in Fig. 10. All templates were matched correctly for SNR > 25 dB. As the SNR decreases, the number of errors increases, reaching 53% if SNR = 0 dB.

In the last experiment, we investigated the influence of the template size on the success rate and the computation time of the ID. We fixed  $\sigma = 2$  while the template size changed from  $64 \times 64$  to  $8 \times 8$  pixels. To make the comparison fair,

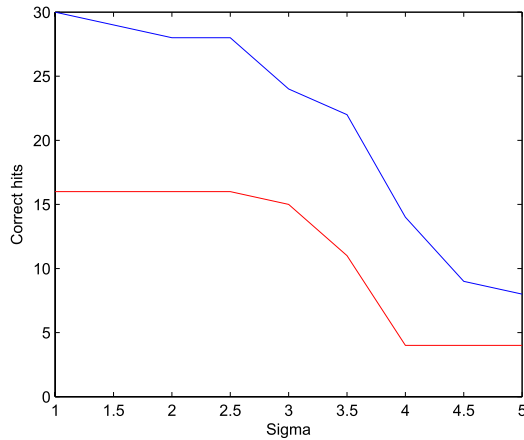


Fig. 9. The number of correctly located templates as a function of the blur size in the noise-free case (blue curve) and in the noisy case (SNR = 0 dB, red curve).

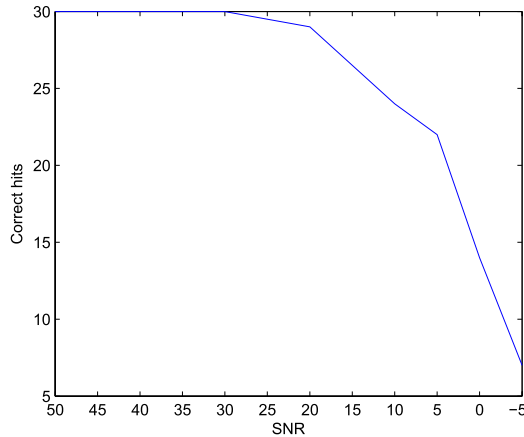


Fig. 10. The number of correctly located blurred templates ( $\sigma = 2$ ) as a function of SNR.

only the positions of the  $64 \times 64$  templates were selected randomly. The smaller templates were obtained by cropping of the largest ones. As one can expect, both the success rate and the computation time decrease along with the decreasing template size (see Table XI, the numbers are means over 5 runs of experiment with 30 templates). The main source of the errors is the boundary effect (which is more significant in small templates since the blur size has been fixed). The time complexity is given by the complexity of moment computation; the calculation of the invariants and the matching itself do not depend on the template size. However, the decrease of the computation time is mild comparing to the rapid increase of the success rate. Taking these two criteria into account simultaneously, one may conclude that in practice large templates should be preferred since they provide better success/speed gain than the small ones.

#### G. Matching of Blurred Templates - Real Blur

Finally, we performed a template matching experiment on astronomical images degraded by real atmospheric turbulence blur. We employed four images of the spot in the solar photosphere taken by a telescope with a CCD camera in a visible spectral band (the venue: Observatory Ondrejov,

TABLE XI  
MATCHING OF BLURRED AND NOISY TEMPLATES BY ID

Template size	Mean time [s]	Correct hits
$64 \times 64$	30.1	30
$32 \times 32$	24.8	27
$16 \times 16$	23.8	16
$8 \times 8$	23.2	2

TABLE XII  
TEMPLATE MATCHING IN ASTRONOMICAL IMAGES

Image	Mean error	Standard deviation	Correct hits
Cross-correlation (CC)			
(b)	7.30	3.82	29
(c)	7.29	3.81	29
(d)	7.28	3.80	28
Zhang distance (ZD)			
(b)	3.73	1.95	28
(c)	3.71	1.94	28
(d)	3.50	1.82	28
Local phase quantization (LPQ)			
(b)	0.87	0.46	30
(c)	0.84	0.44	30
(d)	0.90	0.47	30
Invariant distance (ID)			
(b)	0.88	0.45	30
(c)	0.90	0.47	30
(d)	0.85	0.44	30

Czech Republic; wavelength:  $\lambda \doteq 590$  nm). Since the time interval between the two consecutive acquisitions was only few seconds, the scene can be considered still and the images are almost perfectly registered. As the atmospheric conditions changed between the acquisitions, the amount of blur in individual images vary from one another. We sorted the images according to their blur level by means of the algorithm which compares the energy in low-pass and high-pass wavelet transform bands [66]. The ordered sequence can be seen (and visually checked) in Fig. 11. The size of each image is  $256 \times 256$  pixels. The first image is relatively sharp while the other three images, particularly the last one, are noticeably blurred. The blur kernel is believed to be approximately Gaussian (an experimental validation of this assumption can be found for instance in [72]). Mild additive noise is also present in all images, its estimated SNR is about 30 dB.

By the the four methods used in the previous experiments (CC, ZD, LPQ, and ID), we matched 30 randomly chosen  $32 \times 32$  templates extracted from the first “clear” image against each of the other three images. The maximum order of the invariants used was six. The coarse-to-fine matching algorithm was used with the coarse step 8 pixels and with a  $16 \times 16$  search area on the fine level. For each template, we consider any possible position, we did not apply any restricted search area. This is equivalent to the classification of 30 query images against a database of  $3(256 - 32)^2 = 150528$  images.

As one can see from Table XII, the results are consistent with those we achieved on simulated blurring. The CC localization accuracy is the worst one because of the blur. The Zhang’s distance provides slightly worse accuracy than the invariants. The reason is the presence of noise. Even if the noise is very mild, ZD is highly sensitive to it for the reasons

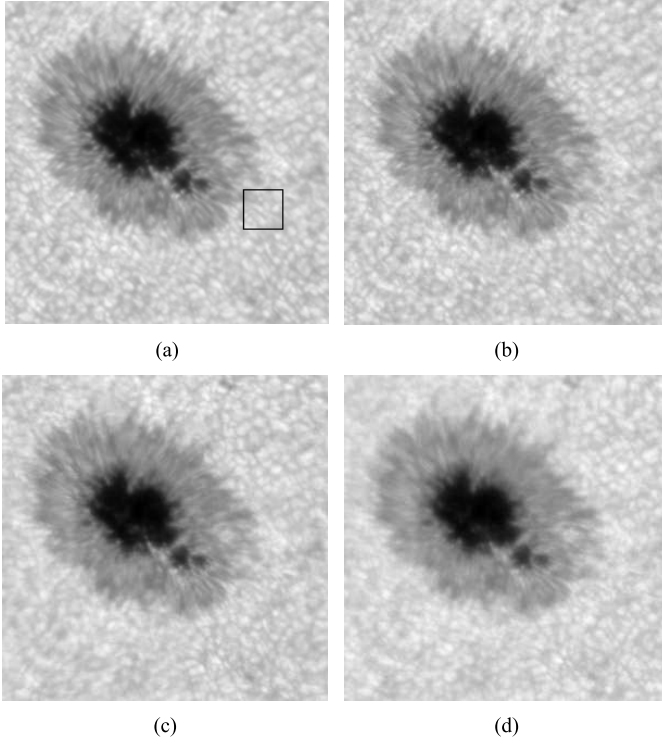


Fig. 11. Four images of the sunspot blurred by atmospheric turbulence blur of various extent. The images are ordered from the less to the most blurred one. One template is depicted in the first image to illustrate its size.

which we already explained in Section IV.D. Both ID and LPQ provides a perfect localization accuracy in this experiment. This is admirable when considering that each template was tested against 150,528 possible positions and that many of them have a very similar visual appearance.

## V. CONCLUSION

We proposed new invariants w.r.t. Gaussian blur, both in frequency and image domains. We showed the performance of the new method in object recognition and in matching of blurred and noisy templates. Comparing to the Zhang's method [65], which has been the only Gaussian-blur invariant metric so far, the proposed method is significantly faster and more robust to additive noise while its recognition rate in noise-free cases is fully comparable to the Zhang's distance. An additional benefit of the new method is that it can be easily made invariant to translation, rotation, scale, and contrast of the image, which is very important in many applications and which is not the case of the Zhang's method. Last but not least, our method handles also an anisotropic Gaussian blur and is even able to compare images of different sizes.

### APPENDIX A

The proof of the equivalence of Eqs. (15) and (16) is due to induction on  $p$ . For  $p = 0, 1, 2$  the equivalence holds well. Now we show the induction step. To avoid the necessity of discrimination between even and odd  $p$ 's, we use a re-indexing in the sums. Introducing  $K = \lceil p/2 \rceil$  and, for simplicity,

$m = m_2/m_0$  we have for Eq. (15)

$$\begin{aligned}
 B(p) &= m_p - \sum_{k=1}^K (2k-1)!! \cdot \binom{p}{2k} m^k B(p-2k) \\
 &= m_p - \sum_{k=1}^K (2k-1)!! \cdot \binom{p}{2k} m^k \sum_{j=0}^{K-k} (2j-1)!! \\
 &\quad \times \binom{p-2k}{2j} (-m)^j m_{p-2k-2j} \\
 &= m_p - \sum_{k=1}^K \sum_{j=0}^{K-k} (-1)^j \frac{p!}{2^{k+j} k! j! (p-2k-2j)!} m^{k+j} \\
 &\quad \times m_{p-2k-2j} \\
 &= m_p - \sum_{k=1}^K \sum_{j=k}^K (-1)^{j-k} \frac{p!}{2^j k! (j-k)! (p-2j)!} m^j \\
 &\quad \times m_{p-2j} \\
 &= m_p - \sum_{j=1}^K \sum_{k=1}^j (-1)^{j-k} \frac{p!}{2^j k! (j-k)! (p-2j)!} m^j \\
 &\quad \times m_{p-2j} \\
 &= m_p - \sum_{j=1}^K (-1)^j \frac{p!}{2^j (p-2j)!} m^j m_{p-2j} \sum_{k=1}^j \frac{(-1)^k}{k! (j-k)!}.
 \end{aligned}$$

Since

$$\sum_{k=1}^j (-1)^k \cdot \binom{j}{k} = -1$$

for any  $j$ , we obtain

$$\begin{aligned}
 B(p) &= m_p + \sum_{j=1}^K (2j-1)!! \binom{p}{2j} (-m)^j m_{p-2j} \\
 &= \sum_{j=0}^K (2j-1)!! \binom{p}{2j} (-m)^j m_{p-2j},
 \end{aligned}$$

which exactly matches Eq. (16).

### APPENDIX B

Let us introduce a vector notation

$$\begin{aligned}
 |\mathbf{p}| &\equiv \sum_{i=1}^N p_i, & \binom{\mathbf{p}}{\mathbf{k}} &\equiv \prod_{i=1}^N \binom{p_i}{k_i}, \\
 \mathbf{p}^{\mathbf{k}} &\equiv \prod_{i=1}^N p_i^{k_i}, & \mathbf{p}!! &\equiv \prod_{i=1}^N p_i!!, \\
 \mathbf{0} &\equiv (0, 0, \dots, 0), & \mathbf{1} &\equiv (1, 1, \dots, 1).
 \end{aligned}$$

The moment of function  $f(\mathbf{x})$  is given as

$$m_{\mathbf{p}} = \int (\mathbf{x} - \mathbf{c})^{\mathbf{p}} f(\mathbf{x}) d\mathbf{x}. \quad (33)$$

The moment of a Gaussian kernel with a diagonal covariance matrix  $\Sigma = \text{diag}(\sigma_1^2, \sigma_2^2, \dots, \sigma_N^2)$  is, in the case that all elements of  $\mathbf{p}$  are even, given as

$$m_{\mathbf{p}} = \sigma^{\mathbf{p}} (\mathbf{p} - \mathbf{1})!! \quad (34)$$

where  $\sigma \equiv (\sigma_1, \sigma_2, \dots, \sigma_N)$ . All other moments are zero. Then we can define an  $N$ -dimensional projection operator

$$P_G(f)(\mathbf{x}) = m_0 G_S(\mathbf{x}),$$

where

$$S = \text{diag}(\mathbf{m}_2/m_0)$$

and

$$\mathbf{m}_2 \equiv (m_{20\dots 0}, m_{02\dots 0}, \dots, m_{00\dots 2}).$$

The  $N$ -D versions of the invariants (15) and (16) are

$$\begin{aligned} B(\mathbf{p}) &= m_{\mathbf{p}} - \sum_{\substack{\mathbf{k}=\mathbf{0} \\ 0 < |\mathbf{k}|}}^{\mathbf{p}} (\mathbf{k} - \mathbf{1})!! \cdot \binom{\mathbf{p}}{\mathbf{k}} (\mathbf{m}_2/m_0)^{\mathbf{k}} B(\mathbf{p} - \mathbf{k}) \\ &= \sum_{\mathbf{k}=\mathbf{0}}^{\mathbf{p}} (\mathbf{k} - \mathbf{1})!! \cdot \binom{\mathbf{p}}{\mathbf{k}} (-1)^{|\mathbf{k}|} (\mathbf{m}_2/m_0)^{\mathbf{k}} m_{\mathbf{p}-2\mathbf{k}}, \quad (35) \end{aligned}$$

where the summation goes over those multi-indices  $\mathbf{k}$  all elements of which are even.

We can do the same even if  $\Sigma$  is not diagonal but the directions of its eigenvectors must be known. The formula for the invariants would, however, look much more complicated. If the eigenvectors of  $\Sigma$  are not known, we cannot properly “rotate” the image, the projection operators cannot be defined and the derivation of the invariants fails.

#### ACKNOWLEDGMENT

We thank the authors of the paper [65] for providing the implementation of their method for comparison, Dr. Stanislava Šimberova for providing the astronomical test images used in the template matching experiment, and Dr. Jaroslav Kautsky for his advice concerning numerical implementation of moments. Sajad Farokhi thanks the Czech Academy of Sciences for the post-doctoral scholarship covering his one-year stay at the Institute of Information Theory and Automation in Prague.

#### REFERENCES

- [1] B. Honarvar, R. Paramesran, and C.-L. Lim, “Image reconstruction from a complete set of geometric and complex moments,” *Signal Process.*, vol. 98, pp. 224–232, May 2014.
- [2] B. Honarvar and J. Flusser, “Image deconvolution in moment domain,” in *Moments and Moment Invariants—Theory and Applications*, G. A. Papakostas, Ed. Xanthi, Greece: Science Gate Publishing, 2014, pp. 111–125.
- [3] A. S. Carasso, “The APEX method in image sharpening and the use of low exponent Lévy stable laws,” *SIAM J. Appl. Math.*, vol. 63, no. 2, pp. 593–618, 2003.
- [4] J. H. Elder and S. W. Zucker, “Local scale control for edge detection and blur estimation,” *IEEE Trans. Pattern Anal. Mach. Intell.*, vol. 20, no. 7, pp. 699–716, Jul. 1998.
- [5] W. Zhang and W.-K. Cham, “Single-image refocusing and defocusing,” *IEEE Trans. Image Process.*, vol. 21, no. 2, pp. 873–882, Feb. 2012.
- [6] F. Xue and T. Blu, “A novel SURE-based criterion for parametric PSF estimation,” *IEEE Trans. Image Process.*, vol. 24, no. 2, pp. 595–607, Feb. 2015.
- [7] J. Flusser, T. Suk, and S. Saic, “Recognition of blurred images by the method of moments,” *IEEE Trans. Image Process.*, vol. 5, no. 3, pp. 533–538, Mar. 1996.
- [8] J. Flusser and T. Suk, “Degraded image analysis: An invariant approach,” *IEEE Trans. Pattern Anal. Mach. Intell.*, vol. 20, no. 6, pp. 590–603, Jun. 1998.
- [9] V. Ojansivu, “Blur invariant pattern recognition and registration in the Fourier domain,” Ph.D. dissertation, Dept. Electr. Inf. Eng., Univ. Oulu, Oulu, Finland, 2009.
- [10] Y. Bentoutou, N. Taleb, K. Kpalma, and J. Ronsin, “An automatic image registration for applications in remote sensing,” *IEEE Trans. Geosci. Remote Sens.*, vol. 43, no. 9, pp. 2127–2137, Sep. 2005.
- [11] Z. Liu, J. An, and L. Li, “A two-stage registration algorithm for oil spill aerial image by invariants-based similarity and improved ICP,” *Int. J. Remote Sens.*, vol. 32, no. 13, pp. 3649–3664, 2011.
- [12] X. Q. Huang, Y.-M. Xiong, M. Z. W. Liao, and W. F. Chen, “Accurate point matching based on combined moment invariants and their new statistical metric,” in *Proc. Int. Conf. Wavelet Anal. Pattern Recognit. (ICWAPR)*, Nov. 2007, pp. 376–381.
- [13] Y. Bentoutou, N. Taleb, M. C. El Mezouar, M. Taleb, and J. Jetto, “An invariant approach for image registration in digital subtraction angiography,” *Pattern Recognit.*, vol. 35, no. 12, pp. 2853–2865, Dec. 2002.
- [14] Y. Bentoutou and N. Taleb, “Automatic extraction of control points for digital subtraction angiography image enhancement,” *IEEE Trans. Nucl. Sci.*, vol. 52, no. 1, pp. 238–246, Feb. 2005.
- [15] Y. Bentoutou and N. Taleb, “A 3-D space–time motion detection for an invariant image registration approach in digital subtraction angiography,” *Comput. Vis. Image Understand.*, vol. 97, no. 1, pp. 30–50, Jan. 2005.
- [16] Y. Zhang, C. Wen, and Y. Zhang, “Estimation of motion parameters from blurred images,” *Pattern Recognit. Lett.*, vol. 21, no. 5, pp. 425–433, May 2000.
- [17] Y. Zhang, C. Wen, Y. Zhang, and Y. C. Soh, “Determination of blur and affine combined invariants by normalization,” *Pattern Recognit.*, vol. 35, no. 1, pp. 211–221, Jan. 2002.
- [18] J. Lu and Y. Yoshida, “Blurred image recognition based on phase invariants,” *IEICE Trans. Fundam. Electron., Commun. Comput. Sci.*, vol. E82-A, no. 8, pp. 1450–1455, 1999.
- [19] X.-J. Shen and J.-M. Pan, “Monocular visual servoing based on image moments,” *IEICE Trans. Fundam. Electron., Commun. Comput. Sci.*, vol. E87-A, no. 7, pp. 1798–1803, 2004.
- [20] B. Mahdian and S. Saic, “Detection of copy–move forgery using a method based on blur moment invariants,” *Forensic Sci. Int.*, vol. 171, nos. 2–3, pp. 180–189, Sep. 2007.
- [21] B. Mahdian and S. Saic, “Detection of near-duplicated image regions,” in *Computer Recognition Systems 2 (Advances in Soft Computing)*, vol. 45. Berlin, Germany: Springer, 2007, pp. 187–195.
- [22] L. Li and G. Ma, “Recognition of degraded traffic sign symbols using PNN and combined blur and affine invariants,” in *Proc. 4th Int. Conf. Natural Comput. (ICNC)*, vol. 3, Oct. 2008, pp. 515–520.
- [23] L. Li and G. Ma, “Optimizing the performance of probabilistic neural networks using PSO in the task of traffic sign recognition,” in *Proc. 4th Int. Conf. Intell. Comput. Adv. Intell. Comput. Theories Appl. Aspects Artif. Intell. (ICIC)*, vol. LNAI 5227, 2008, pp. 90–98.
- [24] Y. Zhang, C. Wen, and Y. Zhang, “Neural network based classification using blur degradation and affine deformation invariant features,” in *Proc. 13th Int. Florida Artif. Intell. Res. Soc. Conf. (FLAIRS)*, 2000, pp. 76–80.
- [25] C. Guang-Sheng and Z. Peng, “Dynamic wood slice recognition using image blur information,” *Sens. Actuators A, Phys.*, vol. 176, pp. 27–33, Apr. 2012.
- [26] J. Flusser, T. Suk, and B. Zitová, “On the recognition of wood slices by means of blur invariants,” *Sens. Actuators A, Phys.*, vol. 198, pp. 113–118, Aug. 2013.
- [27] P. Zhao, “Dynamic timber cell recognition using two-dimensional image measurement machine,” *AIP Rev. Sci. Instrum.*, vol. 82, no. 8, p. 083703, 2011.
- [28] J. Flusser and B. Zitová, “Combined invariants to linear filtering and rotation,” *Int. J. Pattern Recognit. Artif. Intell.*, vol. 13, no. 8, pp. 1123–1136, 1999.
- [29] J. Flusser, B. Zitová, and T. Suk, “Invariant-based registration of rotated and blurred images,” in *Proc. Int. Geosci. Remote Sens. Symp. (IGARSS)*, Jun. 1999, pp. 1262–1264.
- [30] B. Zitová and J. Flusser, “Estimation of camera planar motion from blurred images,” in *Proc. Int. Conf. Image Process. (ICIP)*, vol. 2, 2002, pp. II-329–II-332.
- [31] T. Suk and J. Flusser, “Combined blur and affine moment invariants and their use in pattern recognition,” *Pattern Recognit.*, vol. 36, no. 12, pp. 2895–2907, Dec. 2003.
- [32] Y. Li, H. Chen, J. Zhang, and P. Qu, “Combining blur and affine moment invariants in object recognition,” *Proc. SPIE* vol. 5253, p. 165, Sep. 2003.

- [33] R. Palaniappan, M. P. Paulraj, S. Yaacob, and M. S. Z. Azalan, "A simple sign language recognition system using affine moment blur invariant features," in *Proc. Int. Postgraduate Conf. Eng. (IPCE)*, 2010, p. 5.
- [34] Y. Gao, H. Song, X. Tian, and Y. Chen, "Identification algorithm of winged insects based on hybrid moment invariants," in *Proc. 1st Int. Conf. Bioinform. Biomed. Eng. (iCBBE)*, vol. 2, Jul. 2007, pp. 531–534.
- [35] H. Ji, J. Zhu, and H. Zhu, "Combined blur and RST invariant digital image watermarking using complex moment invariants," in *Proc. 2nd Int. Conf. Signals, Circuits Syst. (SCS)*, Shanghai, China, Nov. 2008, pp. 1–6.
- [36] H. Zhang, H. Shu, G. N. Han, G. Coatrieux, L. Luo, and J. L. Coatrieux, "Blurred image recognition by Legendre moment invariants," *IEEE Trans. Image Process.*, vol. 19, no. 3, pp. 596–611, Mar. 2010.
- [37] C.-Y. Wee and R. Paramesran, "Derivation of blur-invariant features using orthogonal Legendre moments," *IET Comput. Vis.*, vol. 1, no. 2, pp. 66–77, Jun. 2007.
- [38] X. Dai, H. Zhang, H. Shu, and L. Luo, "Image recognition by combined invariants of Legendre moment," in *Proc. IEEE Int. Conf. Inf. Autom. (ICIA)*, Jun. 2010, pp. 1793–1798.
- [39] X. Dai, H. Zhang, H. Shu, L. Luo, and T. Liu, "Blurred image registration by combined invariant of Legendre moment and Harris–Laplace detector," in *Proc. 4th Pacific-Rim Symp. Image Video Technol. (PSIVT)*, Nov. 2010, pp. 300–305.
- [40] H. Zhu, M. Liu, H. Ji, and Y. Li, "Combined invariants to blur and rotation using Zernike moment descriptors," *Pattern Anal. Appl.*, vol. 13, no. 3, pp. 309–319, Aug. 2010.
- [41] B. Chen, H. Shu, H. Zhang, G. Coatrieux, L. Luo, and J. L. Coatrieux, "Combined invariants to similarity transformation and to blur using orthogonal Zernike moments," *IEEE Trans. Image Process.*, vol. 20, no. 2, pp. 345–360, Feb. 2011.
- [42] H. Ji and H. Zhu, "Degraded image analysis using Zernike moment invariants," in *Proc. Int. Conf. Acoust., Speech Signal Process. (ICASSP)*, Apr. 2009, pp. 1941–1944.
- [43] Q. Li, H. Zhu, and Q. Liu, "Image recognition by combined affine and blur Tchebichef moment invariants," in *Proc. 4th Int. Conf. Image Signal Process. (CISP)*, Oct. 2011, pp. 1517–1521.
- [44] X. Zuo, X. Dai, and L. Luo, "M-SIFT: A new descriptor based on Legendre moments and SIFT," in *Proc. 3rd Int. Conf. Mach. Vis. ICMV*, 2010, pp. 183–186.
- [45] D. G. Lowe, "Distinctive image features from scale-invariant keypoints," *Int. J. Comput. Vis.*, vol. 60, no. 2, pp. 91–110, 2004.
- [46] J. Kautsky and J. Flusser, "Blur invariants constructed from arbitrary moments," *IEEE Trans. Image Process.*, vol. 20, no. 12, pp. 3606–3611, Dec. 2011.
- [47] V. Ojansivu and J. Heikkilä, "A method for blur and affine invariant object recognition using phase-only bispectrum," in *Proc. Int. Conf. Image Anal. Recognit. (ICIAR)*, vol. LNCS 5112, 2008, pp. 527–536.
- [48] V. Ojansivu and J. Heikkilä, "Image registration using blur-invariant phase correlation," *IEEE Signal Process. Lett.*, vol. 14, no. 7, pp. 449–452, Jul. 2007.
- [49] S. Tang, Y. Wang, and Y.-W. Chen, "Blur invariant phase correlation in X-ray digital subtraction angiography," in *Proc. IEEE/CME Int. Conf. Complex Med. Eng.*, May 2007, pp. 1715–1719.
- [50] M. Pedone, J. Flusser, and J. Heikkilä, "Blur invariant translational image registration for  $N$ -fold symmetric blurs," *IEEE Trans. Image Process.*, vol. 22, no. 9, pp. 3676–3689, Sep. 2013.
- [51] M. Pedone, J. Flusser, and J. Heikkilä, "Registration of images with  $N$ -fold dihedral blur," *IEEE Trans. Image Process.*, vol. 24, no. 3, pp. 1036–1045, Mar. 2015.
- [52] V. Ojansivu and J. Heikkilä, "Blur insensitive texture classification using local phase quantization," in *Proc. Congr. Image Signal Process. (CISP)*, vol. LNCS 5099, 2008, pp. 236–243.
- [53] V. Ojansivu, E. Rahtu, and J. Heikkilä, "Rotation invariant local phase quantization for blur insensitive texture analysis," in *Proc. 19th Int. Conf. Pattern Recognit. (ICPR)*, Dec. 2008, pp. 1–4.
- [54] E. Rahtu, J. Heikkilä, V. Ojansivu, and T. Ahonen, "Local phase quantization for blur-insensitive image analysis," *Image Vis. Comput.*, vol. 30, no. 8, pp. 501–512, Aug. 2012.
- [55] T. Ahonen, E. Rahtu, V. Ojansivu, and J. Heikkilä, "Recognition of blurred faces using local phase quantization," in *Proc. 19th Int. Conf. Pattern Recognit. (ICPR)*, Dec. 2008, pp. 1–4.
- [56] J. Flusser, T. Suk, and S. Saic, "Recognition of images degraded by linear motion blur without restoration," *Comput. Suppl.*, vol. 11, pp. 37–51, 1996.
- [57] J. Flusser, T. Suk, and S. Saic, "Image features invariant with respect to blur," *Pattern Recognit.*, vol. 28, no. 11, pp. 1723–1732, Nov. 1995.
- [58] J. Flusser and B. Zitová, "Invariants to convolution with circularly symmetric PSF," in *Proc. 17th Int. Conf. Pattern Recognit. (ICPR)*, Aug. 2004, pp. 11–14.
- [59] J. Flusser, T. Suk, J. Boldyš, and B. Zitová, "Projection operators and moment invariants to image blurring," *IEEE Trans. Pattern Anal. Mach. Intell.*, vol. 37, no. 4, pp. 786–802, Apr. 2015.
- [60] J. Liu and T. Zhang, "Recognition of the blurred image by complex moment invariants," *Pattern Recognit. Lett.*, vol. 26, no. 8, pp. 1128–1138, Jun. 2005.
- [61] B. Xiao, J.-F. Ma, and J.-T. Cui, "Combined blur, translation, scale and rotation invariant image recognition by Radon and pseudo-Fourier–Mellin transforms," *Pattern Recognit.*, vol. 45, no. 1, pp. 314–321, Jan. 2012.
- [62] R. Gopalan, P. Turaga, and R. Chellappa, "A blur-robust descriptor with applications to face recognition," *IEEE Trans. Pattern Anal. Mach. Intell.*, vol. 34, no. 6, pp. 1220–1226, Jun. 2012.
- [63] J. Flusser, T. Suk, and B. Zitová, *Moments and Moment Invariants in Pattern Recognition*. Chichester, U.K.: Wiley, 2009.
- [64] Z. Zhang, E. Klassen, A. Srivastava, P. Turaga, and R. Chellappa, "Blurring-invariant Riemannian metrics for comparing signals and images," in *Proc. IEEE Int. Conf. Comput. Vis. (ICCV)*, Nov. 2011, pp. 1770–1775.
- [65] Z. Zhang, E. Klassen, and A. Srivastava, "Gaussian blurring-invariant comparison of signals and images," *IEEE Trans. Image Process.*, vol. 22, no. 8, pp. 3145–3157, Aug. 2013.
- [66] J. Kautsky, J. Flusser, B. Zitová, and S. Šimberová, "A new wavelet-based measure of image focus," *Pattern Recognit. Lett.*, vol. 23, no. 14, pp. 1785–1794, Dec. 2002.
- [67] J. Flusser, "On the independence of rotation moment invariants," *Pattern Recognit.*, vol. 33, no. 9, pp. 1405–1410, Sep. 2000.
- [68] H. R. Sheikh, M. F. Sabir, and A. C. Bovik, "A statistical evaluation of recent full reference image quality assessment algorithms," *IEEE Trans. Image Process.*, vol. 15, no. 11, pp. 3440–3451, Nov. 2006.
- [69] E. C. Larson and D. M. Chandler, "Most apparent distortion: Full-reference image quality assessment and the role of strategy," *J. Electron. Imag.*, vol. 19, no. 1, pp. 011006-1–011006-21, Jan. 2010.
- [70] S. Z. Li, Z. Lei, and M. Ao, "The HFB face database for heterogeneous face biometrics research," in *Proc. IEEE Comput. Soc. Conf. Comput. Vis. Pattern Recognit. Workshops (CVPR Workshops)*, Jun. 2009, pp. 1–8.
- [71] D. Yi, R. Liu, R. Chu, Z. Lei, and S. Z. Li, "Face matching between near infrared and visible light images," in *Proc. Int. Conf. Adv. Biometrics (ICB)*, Aug. 2007, pp. 523–530.
- [72] F. Šroubek and J. Flusser, "Multichannel blind iterative image restoration," *IEEE Trans. Image Process.*, vol. 12, no. 9, pp. 1094–1106, Sep. 2003.



**Jan Flusser** (M'93–SM'03) received the M.Sc. degree in mathematical engineering from Czech Technical University, Prague, Czech Republic, in 1985, the Ph.D. degree in computer science from the Czechoslovak Academy of Sciences, in 1990, and the D.Sc. degree in technical cybernetics in 2001. From 1995 to 2007, he was the Head of the Department of Image Processing. Since 1985, he has been with the Institute of Information Theory and Automation, Czech Academy of Sciences. Since 2007, he has been

the Director of the Institute of Information Theory and Automation. He is currently a Full Professor of Computer Science with the Faculty of Nuclear Science and Physical Engineering, Czech Technical University, and the Faculty of Mathematics and Physics, Charles University, Prague, where he gives undergraduate and graduate courses on digital image processing, pattern recognition, and moment invariants and wavelets. He has authored or co-authored over 200 research publications in his research areas, including the monographs *Moments and Moment Invariants in Pattern Recognition* (Wiley, 2009) and *2D and 3D Image Analysis by Moments* (Wiley, 2016). His research interest covers moments and moment invariants, image registration, image fusion, multichannel blind deconvolution, and superresolution imaging. In 2007, he received the Award of the Chairman of the Czech Science Foundation for the best research project and won the Prize of the Academy of Sciences of the Czech Republic for the contribution to image fusion theory. In 2010, he also received by the SCOPUS 1000 Award. He received the Felber Medal of the Czech Technical University for excellent contribution to research and education in 2015.



**Sajad Farokhi** received the M.Sc. degree in mathematics from Payame Noor University, Shiraz, Iran, in 2011, and the Ph.D. degree in computer science from the Malaysia University of Technology, Johor Bahru, Malaysia, in 2014. He received the Post-Doctoral Fellowship in computer science from the Malaysia University of Technology in 2014 and the Czech Academy of Sciences in image processing from 2014 to 2015. He spent this fellowship at the Institute of Information Theory and Automation, Prague, Czech Republic. His research interests include, namely, invariants, face recognition, and near-infrared image processing.



**Cyril Höschl IV**, received the M.Sc. degree in computer science from the Faculty of Mathematics and Physics, Charles University, Prague, in 2010. He is currently pursuing the Ph.D. degree with the Institute of Information Theory and Automation, Prague, Czech Republic, under the supervision of J. Flusser. His research interests include invariants, moments, shape decomposition methods, mobile programming, and visualization of social interactions (sociomapping).



**Tomáš Suk** received the M.Sc. degree in electrical engineering from the Faculty of Electrical Engineering, Czech Technical University, Prague, Czech Republic, in 1987, and the Ph.D. degree in computer science from the Czechoslovak Academy of Sciences, in 1992. Since 1991, he has been a Researcher with the Institute of Information Theory and Automation, Czech Academy of Sciences, Prague. He has authored 15 journal papers and more than 30 conference papers. He has co-authored the monographs *Moments and Moment Invariants in Pattern Recognition* (Wiley, 2009) and *2D and 3D Image Analysis by Moments* (Wiley, 2016). His research interests include digital image processing, pattern recognition, image filtering, invariant features, moment-based and point-based invariants, spatial transformations of images, and applications in remote sensing, astronomy, botany, medicine, and computer vision. In 2002, he received the Otto Wichterle Premium of the Czech Academy of Sciences for excellent young scientists.



**Barbara Zitová** received the M.Sc. degree in computer science and the Ph.D. degree in software systems from Charles University, Prague, Czech Republic, in 1995 and 2000, respectively. Since 1995, she has been with the Institute of Information Theory and Automation, Czech Academy of Sciences. Since 2008, she has been the Head of the Department of Image Processing. She gives undergraduate and graduate courses on digital image processing and wavelets in image processing with Czech Technical University and the Charles University. Her research interests include geometric invariants, image enhancement, image registration and image fusion, and image processing applications in cultural heritage. She has authored/co-authored over 50 research publications in these areas, including the monographs *Moments and Moment Invariants in Pattern Recognition* (Wiley, 2009), *2D and 3D Image Analysis by Moments* (Wiley, 2016), and tutorials at major conferences. In 2003, she received the Josef Hlavka Student Prize, the Otto Wichterle Premium of the Czech Academy of Sciences for excellent young scientists in 2006, and the SCOPUS 1000 Award for more than 1000 citations of a single paper in 2010.



**Matteo Pedone** received the M.Sc. degree in computer science from the La Sapienza University of Rome, Italy, in 2007, and the Ph.D. degree in computer science from the University of Oulu, Finland, in 2015. He is currently a Post-Doctoral Researcher with the Center for Machine Vision Research, University of Oulu. His research interests include computer vision, computational photography, invariant theory, statistical signal processing, differential geometry, and Clifford algebra.